ACS APPLIED MATERIALS & INTERFACES

Research Article

Cite This: ACS Appl. Mater. Interfaces 2019, 11, 20574−20580

www.acsami.org

Anisotropic Sliding of Underwater Bubbles On Microgrooved Slippery Surfaces by One-Step Femtosecond Laser Scanning

Xiaodong Lv,[†,§] Yunlong Jiao,[‡,§] Sizhu Wu,[*,†] Chuanzong Li,[†] Yiyuan Zhang,[‡] Jiawen Li,[‡] Yanlei Hu,[‡] and Dong Wu[*,‡]

[†]School of Instrument Science and Opto-electronics Engineering, Hefei University of Technology, Hefei 230009, China

[‡]CAS Key Laboratory of Mechanical Behavior and Design of Materials, Department of Precision Machinery and Precision Instrumentation, University of Science and Technology of China, Hefei 230026, China

Supporting Information

ABSTRACT: Slippery liquid-infused surfaces (SLIPS) with excellent liquid sliding abilities have attracted great attention due to their multifunctions in broad fields. However, current research is mainly concentrated on the isotropic SLIPS, and there are few studies about the fabrication of anisotropic SLIPS and the investigation of anisotropic bubble sliding. Herein, we reported a kind of distinct periodic microgrooved slippery surface (MGSS) by one-step femtosecond laser scanning and realized bubble anisotropic sliding in a liquid system. The MGSS enables the bubble to slide along the direction of grooves but prevents the bubble from sliding along the perpendicular direction to the groove. The mechanism is mainly related to the energy barrier difference caused by the spin-coating oil film thickness and the groove height along the parallel and perpendicular directions. The relationship between the driven force of buoyancy and the resistance of contact angle hysteresis was investigated by theoretical analysis, and the theoretical prediction showed a great adherence with the experimental results. We also studied the influence of laser power and groove period on the degree of anisotropy, and it was found that the groove space has little effect on the degree of anisotropy and the strongest bubble anisotropy can reach nearly 80°. Finally, the MGSS was successfully used in anisotropic bubble transportation on flat and curved surfaces. We believe that such functional surfaces will be promising candidates for manipulating bubble directional sliding behavior and further underwater gas collection.

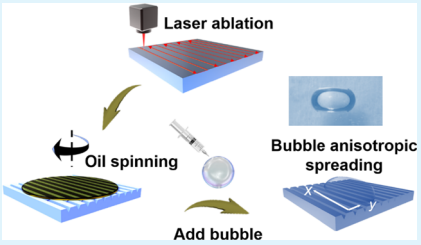

KEYWORDS: *Microgrooved slippery surface, One-step femtosecond laser scanning, Contact angle hysteresis, Anisotropic bubble transportation, Underwater gas directional collection*

1. INTRODUCTION

Inspired by natural carnivorous pitcher plants, different kinds of slippery liquid-infused surfaces (SLIPS) have been researched for many years,[1−4] which consist of a lubricating liquid film locked in place by a porous substrate. Due to their excellent properties of self-cleaning, self-healing, and super-repellency against various liquids,[5−7] SLIPS have been used in lots of applications, such as anti-icing,[8,9] antifouling,[10] anticorrosion,[11] drag reduction,[12] and droplet manipulation.[13,14] For example, Heng et al. fabricated two different kinds of SLIPS by utilizing a reduced graphene oxide film to achieve the manipulation of droplet motion with electric response.[14] Leslie et al. proposed a bioinspired omniphobic surface coating on medical devices to prevent thrombosis and biofouling.[15] Jiang et al. presented a photoelectric cooperative-responsive slippery surface for droplets' multifunctional manipulation.[16] It is worth noting that there were large numbers of studies about droplet transportation on slippery surfaces. Besides, as important components of multiphase systems, slippery surfaces can also be used for the manipulation of bubble movement in a liquid environment, which has tremendous potential applications ranging from catalytic reactions to energy exploration and liquid drug delivery.[17−21] A slippery surface has an adhesion force to bubbles and exhibits easy sliding behavior for bubbles; thus, it is superior to other kinds of interfaces in bubble transportation systems. Jiang and co-workers investigated the sliding behavior of underwater bubbles on the paper-based slippery surface from various perspectives, such as the slant angle of surface, volume of bubbles, and track width.[17] Wang et al. proposed a geometry-gradient lubricant surface for on-demand bubble transportation,[18] which realizes bubble transportation against buoyancy.[19] Guo et al. realized magnetically controllable bubble manipulation on amphibious slippery gel surfaces, which introduced a new way of designing amphibious surfaces for smart control over the sliding behaviors of bubbles underwater.[20] Recently, Jiao et al. fabricated a kind of microtextured slippery surface by laser irradiation and superhydrophobic treatment, and they deeply investigated the influence of the lubricant viscosity on the underwater bubbles sliding in a liquid system.[21] However, it is worth noting that present works are mainly concentrated on the

Received: April 19, 2019
Accepted: May 13, 2019
Published: May 15, 2019

DOI: 10.1021/acsami.9b06849
ACS Appl. Mater. Interfaces 2019, 11, 20574−20580

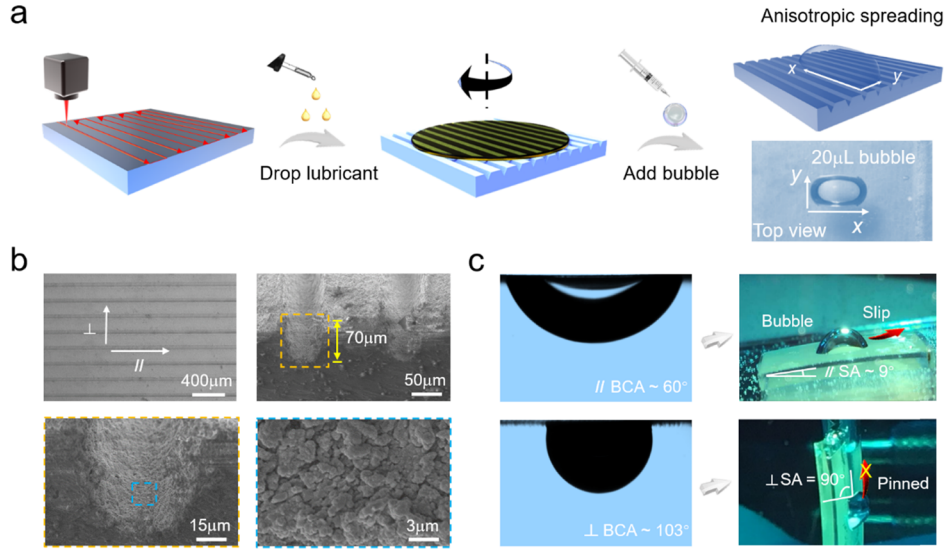

Figure 1. Fabrication procedure of the MGSS and its anisotropic sliding behavior of bubble underwater. (a) Detailed process of preparing MGSS inspired from pitcher plants, including two main steps of laser scanning and lubrication. (b) SEM images of the microgrooves (space ~150 μm, depth ~70 μm) with different magnifications. (c) Side view of contact angles along the parallel and perpendicular directions of a 20 μL bubble underwater and its sliding behavior.

isotropic SLIPS for bubble manipulation,[17,20,21] and there are few studies about the fabrication of anisotropic SLIPS. It is still challenging to find a more facile and environmental-friendly method to fabricate anisotropic SLIPS without chemical processes. Fortunately, femtosecond laser fabrication is a kind of high-tech approach with high machining precision and low thermal effect, which is widely used to prepare multiscale microstructures with superwetting liquid/bubble wettability for the manipulation of liquid/gas movement.[22−25] However, the anisotropic sliding of underwater bubbles on the anisotropic SLIPS by utilizing femtosecond laser has also been rarely explored, which would restrict their potential application in the fields of bubble directional collection, microfluidics, and so on. Additionally, to achieve progressive practical applications, the influence of the microgroove depth, period, and lubricant film thickness on the degree of anisotropy and the mechanism of bubble interaction with anisotropic slippery surfaces should be further studied.

Here, we fabricated a kind of periodic microgrooved slippery surface (MGSS) by one-step femtosecond laser ablation without superhydrophobic treatment, and the anisotropic sliding of underwater bubbles was achieved on the prepared surface. The experimental results showed that the bubble could slide along the direction of the grooves on the MGSS, but MGSS could prevent the bubble from sliding along the perpendicular direction to the groove. The mechanism of this anisotropic sliding is mainly attributed to the energy barrier difference caused by the oil film thickness and the groove height along the parallel and perpendicular directions. Moreover, it was found that the laser power has an important effect on the degree of anisotropy and the strongest bubble anisotropy can reach nearly 80°. Finally, the MGSS was successfully used in anisotropic bubble transportation on flat and curved surfaces. We believe such functional surfaces will be promising candidates for manipulating bubble sliding behavior in liquid systems, which has many potential applications in gas-directional transportation, gas collection, and so on.

2. RESULTS AND DISCUSSION

To achieve the anisotropic sliding of bubbles, three criteria must be satisfied: (1) the surface must be easy to slide for the bubble; (2) there must be an anisotropic structure to guide the bubble in achieving directional sliding; and (3) it should be in a Wenzel state for the bubble on the MGSS surfaces. In these cases, the bubble would adhere tightly on the surface, and it is influenced by the structure. From these principles, the PDMS substrate with microgroove arrays is prepared using one-step femtosecond laser ablation, as shown in Figure 1a. First, the periodic microgrooves are simply constructed by line-by-line irradiation (scanning speed ~2 mm/s). The laser processing system and optical path can be seen in Figure S1, which have been introduced in our previous studies.[21,26,27] Then the surface is lubricated by silicone oil (100 cst) through spin coating, and a thin oil film forms on the surface. Silicone oil is chosen as the aimed lubricant because of its low surface tension and it is widely used in industry. In this experiment, the original PDMS surface was changed from hydrophobic to superhydrophobic by laser ablation because of the increased surface roughness by the microgrooves.[28] The superhydrophobic capability will make the silicone oil stably on the surface.[29] It can be seen that a 20 μL bubble exhibits anisotropic spreading on the oil-infused microgrooves underwater. Figure 1b shows the topographical features of the laser-induced MGSS (space ~150 μm, depth ~70 μm) at different magnifications. It can be seen that the nanoparticles are randomly located on the surface after laser ablation on account of the interaction between the laser and material. We also fabricated different parameters of microgrooves to further explore the effect of microgroove depth and period on the degree of anisotropy on the MGSS (Figure S2). The parallel contact angle of a 20 μL bubble ($BCA_{//}$ ~60°) along the direction of microgrooves has a great difference with the perpendicular contact angle ($BCA_{\perp}$ ~103°) (Figure 1c). When the MGSS is slightly tilted, bubbles can easily slide along the direction of microgrooves ($SA_{//}$ ~9°, Movie S1). However,

DOI: 10.1021/acsami.9b06849
ACS Appl. Mater. Interfaces 2019, 11, 20574−20580

the bubble is pinned on the MGSS when it is perpendicular to the groove direction ($SA_{\perp}$ ~90°, Movie S2).

To better understand the bubble anisotropic sliding behavior, the mechanism of the bubble transportation on the MGSS is analyzed in Figure 2. It should be noted that the

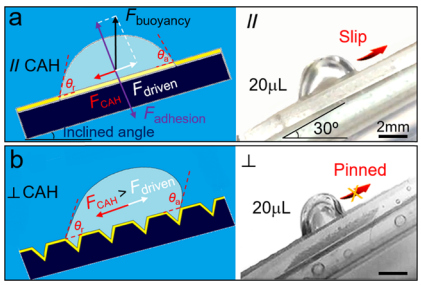

Figure 2. Physical mechanism of anisotropic sliding of bubble underwater on the MGSS. (a) A 20 μL bubble can easily slide upward along the direction parallel to grooves under buoyancy with an inclined angle of about 30°. (b) The bubble is pinned on the surface along the perpendicular direction under the same condition because of the increasing resistance. The images on the right are the experimental results.

bubble is in a Wenzel state[30] on the MGSS. As shown in Figure 2a, a 20 μL bubble can move rapidly along the direction of microgrooves under a slope angle of 30°. In contrast, the bubble with the same volume is pinned on the surface when it is perpendicular to the groove direction with the same slope angle (Figure 2b). The driven force of bubble motion is the axis-direction component of buoyancy, which is defined as

$$F_{driven} = \rho \cdot V \cdot g \cdot \sin \alpha \quad (1)$$

where ρ, V, g, and α denote the water density, bubble volume, gravitational acceleration, and tilt angle of surface, respectively.[17] According to eq 1, when a 20 μL bubble slides along the tilted substrate of ~30°, the accurate calculation of F_{driven} is 9.8×10^{-5} N. The adhesion force of MGSS guarantees that the bubble is in contact with grooves and is in a Wenzel state. This force is balanced with the component of buoyancy perpendicular to the axial direction. The main motion resistance is the contact angle hysteresis (CAH) of the bubble. The resistance of CAH is calculated as

$$F_{CAH} = \gamma \cdot L \cdot (\cos \theta_r - \cos \theta_a) \quad (2)$$

where γ, L, θ_r, and θ_a represent the surface tension of water, bubble's contact line length, and receding and advancing angles of the bubble, respectively.[13] The experimental results of the contact line length, receding, and advancing angles in Figure 2a are measured about 0.46 cm, 66°, and 80°, respectively. According to eq 2, the $F_{CAH//}$ is calculated about 7.7×10^{-5} N. Besides, the contact line length, receding, and advancing angles in Figure 2b are measured about 0.32 cm, 72°, and 106°, respectively, so the calculated $F_{CAH\perp}$ is about 1.34×10^{-4} N. Apparently, along the perpendicular direction to grooves, the resistance of CAH caused by energy barrier $F_{CAH\perp}$ exceeds F_{driven} ($1.34 \times 10^{-4} > 9.8 \times 10^{-5}$ N), so the bubble cannot slide when the slant angle is nearly 30°. It should be considered that the contact line would pin at the highest energy barrier until the contact line is forced to pass this sticking point.[31] On the contrary, along the parallel direction to grooves, because the resistance of CAH caused by energy barrier $F_{CAH//}$ is smaller than the F_{driven} ($7.7 \times 10^{-5} < 9.8 \times 10^{-5}$ N), so the bubble is prone to move in the direction of grooves. It is worth noting that the experimental results have a great adherence of the theoretical prediction.

The bubble anisotropic sliding behavior is closely related to the oil film thickness on the MGSS. It should be pointed out that the oil film thickness is the distance between the upper surface of the oil film and top of grooves and it is approximatively measured by the microscope. The detailed measurement strategy of oil film thickness is shown in the Supporting Information. As a matter of fact, the film thickness is mainly influenced by two factors under spin coating. One is the rotation speed of the spin coater, and the other is rotation time. It is worth pointing out that the oil film thickness during this experiment is controlled by adjusting the rotation time at a constant rotation speed (1500 r/min). The oil film thickness and its variation with spin time are shown in Figure 3a. In the

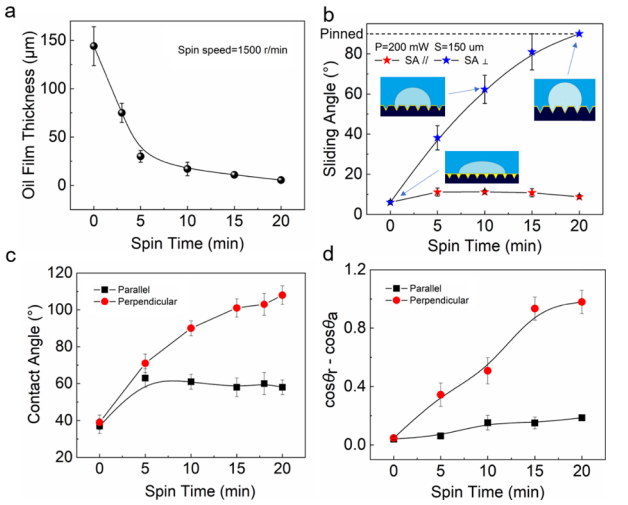

Figure 3. (a) Relationship between the spin time and oil film thickness. (b) Different sliding angles along the parallel and perpendicular directions under different oil film thicknesses. (c) Relationship between the CA and the spin time in both directions. (d) Relationship between the CAH ($\cos\theta_r - \cos\theta_a$) and the spin time in both directions.

beginning (<2 s), the silicone oil fully covers the microstructures and forms a thick film of ~150 μm, so the bubble directly contacts with the flat oil film (inset of Figure 3b) with a small CAH. Both the parallel and perpendicular sliding angles of bubbles are close to 6°, which makes the MGSS isotropic. The contact angles in both directions ($CA_{//}$ ~37°, $CA_{\perp}$ ~39°) are almost the same at the beginning of spin time (Figure 3c and Figure S3). With the increase of spin time, the oil film becomes thinner and uneven because of the existence of microgrooved structures (inset of Figure 3b); thus, the bubble shows a high CAH and obvious anisotropic behavior along the perpendicular direction. It can be seen that, when spin time reaches 20 min, the oil film thickness decreases to about 6 μm (Figure 3a) and the bubble shows the strongest anisotropy of ~80°. It slides along the groove direction with a slant angle of 9°, while it is pinned on the surface along the perpendicular direction even when the slant angle reaches 90° (Figure 3b). Similarly, the contact angles in both directions also reach the biggest difference when the spin time comes to 20 min ($CA_{//}$ ~58°, $CA_{\perp}$ ~108°). To further understand the anisotropic spreading behavior of the MGSS with the variation of spin time, we calculated the theoretical value of CAH ($\cos\theta_r$ − cos

DOI: 10.1021/acsami.9b06849
ACS Appl. Mater. Interfaces 2019, 11, 20574−20580

θ_a) along the two directions under different spin times according to eq 2 (Figure 3d). It can be seen that the CAH along the parallel direction to grooves remains constant and the bubble shows a small CAH all the time, while along the perpendicular direction to grooves, the CAH of bubbles increases from 0.05 to 0.97 with the increase of spin time, which is mainly caused by the decrease of oil film thickness. When the oil film becomes thinner, the bubble would directly contact with the uneven film caused by the microgrooves and would show a high CAH. It would be restricted by adjacent microgrooved structures when sliding along the perpendicular direction to grooves, and the bubble shows strongest anisotropy at a spin time of ~20 min. The experimental results have a great coherence with the theoretical prediction.

Additionally, we conducted quantitative research to explore the influence of different groove parameters (depth and period) on the degree of anisotropy. The experimental results show that the anisotropy of underwater bubbles can be controlled by adjusting the laser power and scanning period (Figure 4). The depth of grooves increases with the power of

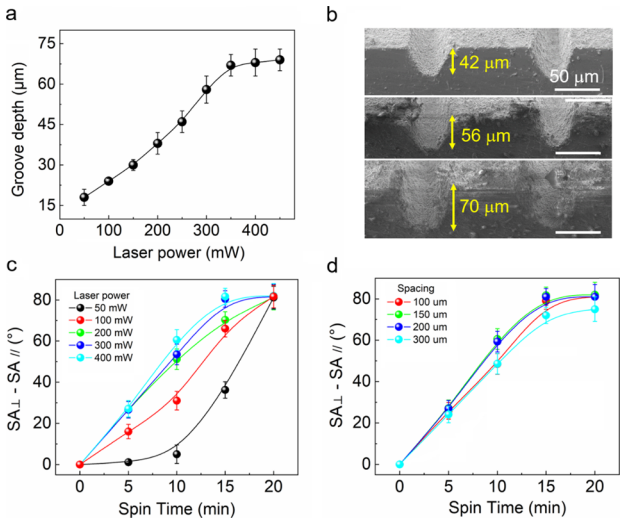

Figure 4. Quantitative research of different parameters associated with anisotropy. (a) Relationship between the laser power and the groove depth. (b) SEM images of the groove depth at different laser powers. (c) Influence of microgroove depth on degree of anisotropy. (d) Influence of microgroove space on degree of anisotropy.

laser ablation, which forms an approximate proportional relationship, as shown in Figure 4a. The MGSSs with different depths (42, 56, 70 μm) were obtained under different powers of laser ablation (200, 300, 400 mW) (Figure 4b). In Figure 4c, the difference in the perpendicular and parallel sliding angles of 20 μL bubbles represents the degree of anisotropy. When the laser power is 50 mW, the groove depth is small (~18 μm) with a low energy barrier. In this case, it needs more spin time (~20 min) to make the oil film interface below the microstructure and to reach the anisotropy. When laser power reaches 400 mW (depth ~70 μm), it only needs 15 min to achieve an obvious degree of anisotropy of about 80°. It can be pointed out that the anisotropy of MGSS increases with the increasing depth of grooves. In addition, the relationship between the degree of anisotropy and the groove space is studied as well (Figure 4d). The results show that the groove space has little effect on the degree of bubble anisotropy on the MGSS, and there exists a similar degree of anisotropy when the groove space increases from 100 to 300 μm, which may probably be because the resistance of CAH is basically the same at different groove period.

To further explore the suitability and durability of MGSS for underwater bubble anisotropic sliding, we conducted a series of repetitive sliding angle (SA) experiments on the MGSS with different types of lubricants and different kinds of liquid systems (Figure 5). It is apparent that all the SAs on the MGSS

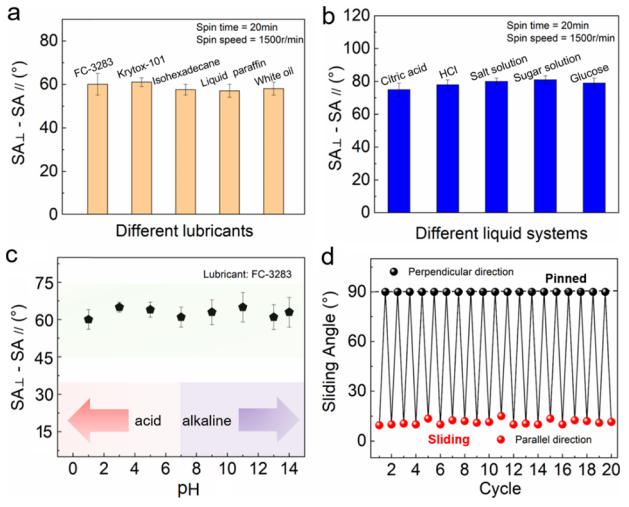

Figure 5. Suitability and durability of MGSS for underwater bubble anisotropic sliding. (a) Degree of anisotropy of MGSS under different lubrication conditions. (b) Degree of anisotropy of MGSS under different liquid systems. (c) Influence of pH on the anisotropic behavior of MGSS. (d) Relationship between the sliding angle and the test recycles.

with different lubricants, such as FC3283, Krytox-101, liquid paraffin, and white oil, show an anisotropic degree of 60° (Figure 5a). The MGSS is also suitable for different kinds of liquid systems (Figure 5b). It can be seen that the bubbles keep an anisotropic degree of ~75° when the liquid system is replaced by citric acid, which shows a great suitability of the anisotropic feature. In addition, the pH of the liquid system has little influence on the anisotropy (Figure 5c), and the bubbles exhibit anisotropic behavior about 60° with the increase of pH from acid (pH ~1) to alkaline (pH ~14). Figure 5d studies the durability of MGSS for underwater bubble anisotropic sliding. It can be seen that the MGSS shows a stable anisotropic sliding ability after several test cycles (20 cycles). However, it is clear that, with the increase of experiment cycles, the loss of lubricant oil existed, which is caused by the interaction between the bubble and the film.[32] To prolong the durability of MGSS for bubble anisotropic sliding, the lubricant on the MGSS should be replenished in time to achieve the continuous anisotropic ability.

Underwater bubble directional manipulation is highly desirable in recent studies. Although it has been researched using different kinds of materials with superwettability, it is still a challenge to achieve on-demand bubble directional transportation on the large-area slippery surface. Therefore, on the basis of anisotropic MGSS, three kinds of L-shaped, curved, and semicircle-shaped MGSSs are prepared by one-step laser linear ablation for on-demand underwater bubble directional manipulation and bubble merging. First, the L-shaped microgrooves are processed (laser power ~400 mW, space ~150 μm) and subsequently spin-coated with silicone oil in 20

DOI: 10.1021/acsami.9b06849
ACS Appl. Mater. Interfaces 2019, 11, 20574−20580

min. After being placed underwater with an inclined angle of about 30° (Figure 6a), bubbles can slide along the 2 cm length

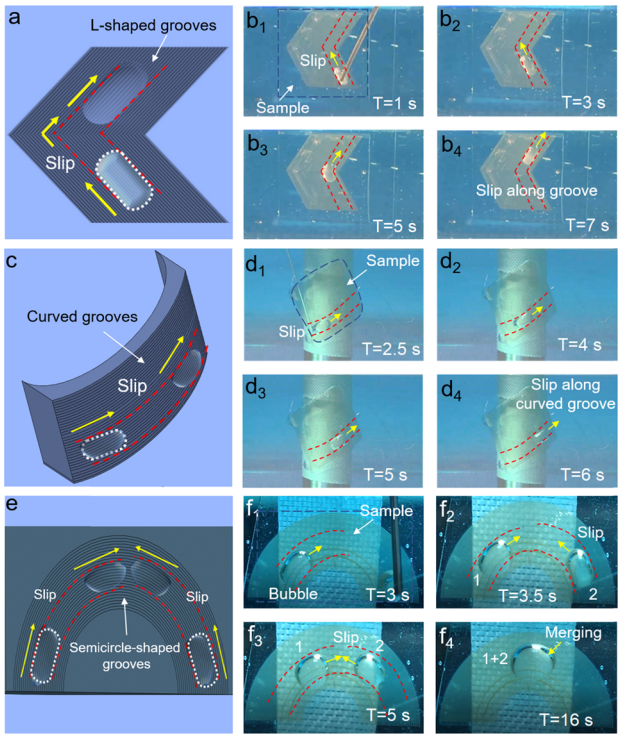

Figure 6. Applications of anisotropic bubble sliding behavior in directional transportation of bubble underwater. (a) Large-area L-shaped microgrooves with an inclined angle of about 30°. (b_1–b_4) The bubble slips upward along grooves in 16 s with an L-shaped track. (c) A large-area curved MGSS is held upright. (d_1–d_4) The bubble moves along microgrooves in 5 s without any displacement in the perpendicular direction. (e) Large-area semicircle-shaped microgrooves on the MGSS. (f_1–f_4) Process of two bubbles merging on the MGSS with semicircle-shaped microgrooves.

L-shaped path precisely in 16 s (Figure 6b and Movie S3). It can be seen clearly that the bubble would not slide perpendicular to the direction of grooves even at the turning point (Figure 6b_1–b_3). It moves along the direction of grooves from beginning to end (Figure 6b_4). Soon afterward, a linear MGSS is ablated using the same parameters, and then it is spin-coated with oil. It is attached on a cylinder so that the MGSS turns into a curved surface (Figure 6c). It is found that the bubble can still slide along the direction of grooves (Movie S4). Because of the high slant angle (90°), the driven force becomes larger so that the bubble moves about 1.5 cm in 5 s (Figure 6d_1–d_4). Finally, we designed a kind of semicircle-shaped groove on the MGSS to achieve the merging of two bubbles from different directions (Figure 6e), which have potential applications in the field of bubble microreactors. It can be seen that, when the first bubble (bubble 1) is dropped on the left bottom of MGSS, it only slides along the circumferential direction under the effect of buoyancy (Figure 6f_1). When the other bubble (bubble 2) is dropped on the right bottom of MGSS (Figure 6f_2), it is also confined in the slippery area and only slides along the circumferential direction. Finally, two bubbles merge into a big bubble at the highest point of the semicircle-shaped grooves (Figure 6f_3,f_4). The detailed merging process is shown in Movie S5. In short, the proposed strategy, which is based on silicone oil infused large-area MGSS, shows powerful bubble anisotropic sliding behavior and may open a new avenue for underwater flammable gas collection, chemical experiments, and transportation systems.

3. CONCLUSIONS

In summary, a kind of distinct slippery periodic microgroove was realized by one-step femtosecond laser ablation for underwater bubble anisotropic sliding. The MGSS enables the bubble to slide along the direction of grooves but prevents the bubble from sliding along the perpendicular direction to the groove. The mechanism of anisotropic behavior is believed as the energy barrier difference caused by the spin-coating oil film thickness and the groove height along the parallel and perpendicular directions. In addition, it is found that the groove space has little effect on the degree of anisotropy and the strongest bubble anisotropy can reach nearly 80°. Finally, the MGSS is successfully applied in anisotropic bubble transportation on flat (L-shaped and semicircle-shaped) and curved surfaces, which could be used for on-demand underwater bubble directional transportation and bubble merging. This novel surface will find wide applications in bubble microreactors, bubble-directional transportation, microfluidics, and related research.

4. EXPERIMENTAL DETAILS

4.1. Materials. The PDMS (Sylgard 184 Kit, Dow Corning) substrate was prepared by mixing the prepolymer and crosslinker at a ratio of 10:1. After degasification for about 30 min, the mixture was poured in a square mold and cured on a heating plate for 0.5 h at 100 °C. Finally, it was cut into pieces (2 × 2 cm^2) for laser processing. The viscosity of silicone fluid (PMX-200, Dow Corning) in this experiment was 100 cst. FC-3283 (viscosity of 0.75 cst at 20 °C) was the 3M Fluorinert electronic liquid. Other lubricants such as Krytox 101 (viscosity of 440 cst at 20 °C; DuPont), liquid paraffin (viscosity of 230 cst at 20 °C), white oil (viscosity of 10 cst at 20 °C), and isohexadecane (viscosity of 3 cst at 20 °C) were also used for this research. Solution mass fractions of citric acid, HCl solution, salt solution, sugar solution, and glucose were 4.07, 5.12, 4.40, 2.37, and 3.0%, respectively. NPT (normal pressure and temperature) air (20 °C, 1 atm, 1.205 × 10^{-3} g/cm^3 density) served as the test material in the underwater contact and sliding angle measurement.

4.2. Microstructure Fabrication. The PDMS substrate was ablated by line-by-line femtosecond laser scanning, and the processing area was 1.5 × 1.5 cm^2. The laser beam (104 fs pulses) with a repetition rate of 1 kHz at a central wavelength of 800 nm from a regenerative amplified Ti:sapphire femtosecond laser system (Legend Elite-1 K-HE, Coherent, USA) was employed for ablation. The laser beam was guided onto the PDMS substrate surface through a galvanometric scanning system (SCANLAB, Germany), which was equipped with a 63 mm telecentric $f\theta$ lens to make the laser beam focus and scan along the x/y coordinate direction. The schematic of the femtosecond laser system and scanning path is shown in Figure S1. The scanning spacing between two adjacent lines ranged from 100 to 300 μm. The laser power ranged from 50 to 400 mW, and the scanning speed was 2 mm/s.

4.3. Spin-Coating Processing. The laser-induced microstructured surface needed to be spun with silicone oil. The spin coater (12A, purchased from Crown Brand Electronic Equipment Factory, Jinan, China) was used in this experiment. The adjustable rotation speed was between 100 and 7000 rpm at factory settings. By adjusting the rotation time from 0 to 20 min at a constant rotation speed (1500 r/min), different oil film thicknesses on microstructures were obtained.

4.4. Instrument and Characterization. Scanning electron microscopy (SEM) photos were utilized to analyze the surface topography of the laser-induced PDMS substrate via use of a field-

DOI: 10.1021/acsami.9b06849
ACS Appl. Mater. Interfaces 2019, 11, 20574–20580

emission scanning electron microscope (JSM-6700F, JEOL, Japan). The contact angles of the bubble underwater were measured on the slippery microstructured surface with a contact angle system (CA100C, Innuo, China). The volume of the air bubble was set to be 20 μL. The average values were obtained by measuring five bubbles at different locations on the same surface. Furthermore, to measure the sliding angle of the air bubble in water, the microstructured surface was slowly tilted with an increment of 2° until the air bubble started to slide. All the contact and sliding angle measurements were conducted under 10% humidity and 20 °C temperature, respectively.

4.5. Underwater Bubble Anisotropic Sliding Strategy. After spin-coating processing, the oil-infused microstructured surface was placed in water. By tilting the surface slowly until the bubble started to slide, bubble sliding angles in parallel and perpendicular directions were measured. After comparing the different anisotropy with different parameters of microstructures and spin times, the strongest anisotropic behavior of bubbles underwater could be discovered.

■ ASSOCIATED CONTENT

Supporting Information

The Supporting Information is available free of charge on the ACS Publications website at DOI: 10.1021/acsami.9b06849.

Laser processing system and optical path; microstructure fabrication; observation of the oil film thickness on microgrooved surfaces; SEM images of the different parameters of microgrooves at different magnifications; variation of bubble contact angles in both directions (parallel and perpendicular direction to grooves) at different spin times (PDF)

20 μL bubble moves on slippery microgrooved surfaces in the groove direction at a tilted angle of 9° (AVI)

20 μL bubble pins on slippery microgrooved surfaces in the direction perpendicular to grooves at a tilted angle of nearly 90° (AVI)

Application of bubble anisotropic sliding on an L-shaped surface (AVI)

Application of bubble anisotropic sliding on a curved surface (AVI)

Application of two bubbles merging on the semicircle-shaped MGSS (AVI)

■ AUTHOR INFORMATION

Corresponding Authors

*E-mail: sizhuwu@hfut.edu.cn (S.W.).

*E-mail: dongwu@ustc.edu.cn (D.W.).

ORCID

Yunlong Jiao: 0000-0001-7718-7342

Jiawen Li: 0000-0003-3950-6212

Yanlei Hu: 0000-0003-1964-0043

Dong Wu: 0000-0003-0623-1515

Author Contributions

§X.L. and Y.J. contributed equally to this work.

Notes

The authors declare no competing financial interest.

■ ACKNOWLEDGMENTS

This work was supported by the National Natural Science Foundation of China (Nos. 51805508, 51875160, 61505047, 51875544, and 61805230), Fundamental Research Funds for the Central Universities (Nos. WK2090090025, JZ2017YY-PY0240), National Key R&D Program of China (2017YFB1104303), and the China Postdoctoral Science Foundation (No. 2018M642534). We acknowledge the Experimental Center of Engineering and Material Sciences at USTC for the fabrication and measuring of samples.

■ REFERENCES

(1) Wong, T.-S.; Kang, S. H.; Tang, S. K. Y.; Smythe, E. J.; Hatton, B. D.; Grinthal, A.; Aizenberg, J. Bioinspired Self-repairing Slippery Surfaces with Pressure-stable Omniphobicity. *Nature* **2011**, *477*, 443−447.

(2) Yao, Y.; Hu, Y.; Grinthal, A.; Wong, T.-S.; Mahadevan, L.; Aizenberg, J. Adaptive Fluid-infused Porous Films with Tunable Transparency and Wettability. *Nat. Mater.* **2013**, *12*, 529−534.

(3) Guo, T.; Che, P.; Heng, L.; Fan, L.; Jiang, L. Anisotropic Slippery Surfaces: Electric-Driven Smart Control of a Drop's Slide. *Adv. Mater.* **2016**, *28*, 6999−7007.

(4) Wang, Z.; Liu, Y.; Guo, P.; Heng, L.; Jiang, L. Photoelectric Synergetic Responsive Slippery Surfaces Based on Tailored Anisotropic Films Generated by Interfacial Directional Freezing. *Adv. Funct. Mater.* **2018**, *28*, 1801310.

(5) Liu, H.; Zhang, P.; Liu, M.; Wang, S.; Jiang, L. Organogel-based Thin Films for Self-Cleaning on Various Surfaces. *Adv. Mater.* **2013**, *25*, 4477−4481.

(6) Tenjimbayashi, M.; Togasawa, R.; Manabe, K.; Matsubayashi, T.; Moriya, T.; Komine, M.; Shiratori, S. Liquid-Infused Smooth Coating with Transparency, Super-Durability, and Extraordinary Hydrophobicity. *Adv. Funct. Mater.* **2016**, *26*, 6693−6702.

(7) Wooh, S.; Vollmer, D. Silicone Brushes: Omniphobic Surfaces with Low Sliding Angles. *Angew. Chem., Int. Ed.* **2016**, *55*, 6822−6824.

(8) Subramanyam, S. B.; Rykaczewski, K.; Varanasi, K. K. Ice Adhesion on Lubricant-impregnated Textured Surfaces. *Langmuir* **2013**, *29*, 13414−13418.

(9) Lv, J.; Song, Y.; Jiang, L.; Wang, J. Bio-Inspired Strategies for Anti-Icing. *ACS Nano* **2014**, *8*, 3152−3169.

(10) Sunny, S.; Vogel, N.; Howell, C.; Vu, T. L.; Aizenberg, J. Lubricant-Infused Nanoparticulate Coatings Assembled by Layer-by-Layer Deposition. *Adv. Funct. Mater.* **2014**, *24*, 6658−6667.

(11) Lee, J.; Shin, S.; Jiang, Y.; Jeong, C.; Stone, H. A.; Choi, C.-H. Oil-Impregnated Nanoporous Oxide Layer for Corrosion Protection with Self-Healing. *Adv. Funct. Mater.* **2017**, *27*, 1606040.

(12) Wang, Y.; Zhang, H.; Liu, X.; Zhou, Z. Slippery Liquid-infused Substrates: A Versatile Preparation, Unique Anti-wetting and Drag-reduction Effect on Water. *J. Mater. Chem. A* **2016**, *4*, 2524−2529.

(13) Wang, Z.; Heng, L.; Jiang, L. Effect of Lubricant Viscosity on the Self-healing Properties and Electrically Driven Sliding of Droplets on Anisotropic Slippery Surfaces. *J. Mater. Chem. A* **2018**, *6*, 3414−3421.

(14) Che, P.; Heng, L.; Jiang, L. Lubricant-Infused Anisotropic Porous Surface Design of Reduced Graphene Oxide Toward Electrically Driven Smart Control of Conductive Droplets' Motion. *Adv. Funct. Mater.* **2017**, *27*, 1606199.

(15) Leslie, D. C.; Waterhouse, A.; Berthet, J. B.; Valentin, T. M.; Watters, A. L.; Jain, A.; Kim, P.; Hatton, B. D.; Nedder, A.; Donovan, K.; Super, E. H.; Howell, C.; Johnson, C. P.; Vu, T. L.; Bolgen, D. E.; Rifai, S.; Hansen, A. R.; Aizenberg, M.; Super, M.; Aizenberg, J.; Ingber, D. E. A Bioinspired Omniphobic Surface Coating on Medical Devices Prevents Thrombosis and Biofouling. *Nat. Biotechnol.* **2014**, *32*, 1134−1140.

(16) Han, K.; Heng, L.; Zhang, Y.; Liu, Y.; Jiang, L. Slippery Surface Based on Photoelectric Responsive Nanoporous Composites with Optimal Wettability Region for Droplets' Multifunctional Manipulation. *Adv. Sci.* **2019**, *6*, 1801231.

(17) Yu, C.; Zhu, X.; Li, K.; Cao, M.; Jiang, L. Manipulating Bubbles in Aqueous Environment via a Lubricant-Infused Slippery Surface. *Adv. Funct. Mater.* **2017**, *27*, 1701605.

(18) Tang, X.; Xiong, H.; Kong, T.; Tian, Y.; Li, W.-D.; Wang, L. Bioinspired Nanostructured Surfaces for On-Demand Bubble Transportation. *ACS Appl. Mater. Interfaces* **2018**, *10*, 3029−3038.

(19) Zhang, C.; Zhang, B.; Ma, H.; Li, Z.; Xiao, X.; Zhang, Y.; Cui, X.; Yu, C.; Cao, M.; Jiang, L. Bioinspired Pressure-Tolerant

Asymmetric Slippery Surface for Continuous Self-Transport of Gas Bubbles in Aqueous Environment. *ACS Nano* **2018**, *12*, 2048−2055.
(20) Guo, P.; Wang, Z.; Heng, L.; Zhang, Y.; Wang, X.; Jiang, L. Magnetocontrollable Droplet and Bubble Manipulation on a Stable Amphibious Slippery Gel Surface. *Adv. Funct. Mater.* **2019**, *29*, 1808717.
(21) Jiao, Y.; Lv, X.; Zhang, Y.; Li, C.; Li, J.; Wu, H.; Xiao, Y.; Wu, S.; Hu, Y.; Wu, D.; Chu, J. Pitcher Plant-bioinspired Bubble Slippery Surface Fabricated by Femtosecond Laser for Buoyancy-driven Bubble Self-transport and Efficient Gas Capture. *Nanoscale* **2019**, *11*, 1370−1378.
(22) Yin, K.; Yang, S.; Dong, X.; Chu, D.; Duan, J.-A.; He, J. Robust Laser-structured Asymmetrical PTFE Mesh for Underwater Directional Transportation and Continuous Collection of Gas Bubbles. *Appl. Phys. Lett.* **2018**, *112*, 243701.
(23) Duan, J.-A.; Dong, X.; Yin, K.; Yang, S.; Chu, D. A Hierarchical Superaerophilic Cone: Robust Spontaneous and Directional Transport of Gas Bubbles. *Appl. Phys. Lett.* **2018**, *113*, 203704.
(24) Yin, K.; Du, H.; Dong, X.; Wang, C.; Duan, J.-A.; He, J. A Simple Way to Achieve Bioinspired Hybrid Wettability Surface with Micro/nanopatterns for Efficient Fog Collection. *Nanoscale* **2017**, *9*, 14620−14626.
(25) Yin, K.; Chu, D.; Dong, X.; Wang, C.; Duan, J.-A.; He, J. Femtosecond Laser Induced Robust Periodic Nanoripple Structured Mesh for Highly Efficient Oil-water Separation. *Nanoscale* **2017**, *9*, 14229−14235.
(26) Jiao, Y.; Li, C.; Wu, S.; Hu, Y.; Li, J.; Yang, L.; Wu, D.; Chu, J. Switchable Underwater Bubble Wettability on Laser-Induced Titanium Multiscale Micro−/Nanostructures by Vertically Crossed Scanning. *ACS Appl. Mater. Interfaces* **2018**, *10*, 16867−16873.
(27) Jiao, Y.; Li, C.; Lv, X.; Zhang, Y.; Wu, S.; Chen, C.; Hu, Y.; Li, J.; Wu, D.; Chu, J. In Situ Tunable Bubble Wettability with Fast Response Induced by Solution Surface Tension. *J. Mater. Chem. A* **2018**, *6*, 20878−20886.
(28) Wu, D.; Wang, J.-N.; Wu, S.-Z.; Chen, Q.-D.; Zhao, S.; Zhang, H.; Sun, H.-B.; Jiang, L. Three-Level Biomimetic Rice-Leaf Surfaces with Controllable Anisotropic Sliding. *Adv. Funct. Mater.* **2011**, *21*, 2927−2932.
(29) Dai, X.; Sun, N.; Nielsen, S. O.; Stogin, B. B.; Wang, J.; Yang, S.; Wong, T.-S. Hydrophilic Directional Slippery Rough Surfaces for Water Harvesting. *Sci. Adv.* **2018**, *4*, No. eaaq0919.
(30) Wenzel, R. N. Resistance of Solid Surfaces to Wetting by Water. *Ind. Eng. Chem.* **1936**, *28*, 988−994.
(31) Chung, J. Y.; Youngblood, J. P.; Stafford, C. M. Anisotropic Wetting on Tunable Micro-Wrinkled Surfaces. *Soft Matter.* **2007**, *3*, 1163−1169.
(32) Kreder, M. J.; Daniel, D.; Tetreault, A.; Cao, Z.; Lemaire, B.; Timonen, J. V. I.; Aizenberg, J. Film Dynamics and Lubricant Depletion by Droplets Moving on Lubricated Surfaces. *Phys. Rev. X* **2018**, *8*, No. 031053.

DOI: 10.1021/acsami.9b06849
ACS Appl. Mater. Interfaces 2019, 11, 20574−20580